J Solid State Electrochem (2012) 16:2383–2389
DOI 10.1007/s10008-012-1756-x

ORIGINAL PAPER

Grain boundary corrosion of the surface of annealed thin layers of gold by OH˙ radicals

Ulrich Hasse · Katja Fricke · Daiane Dias · Gustav Sievers · Harm Wulff · Fritz Scholz

Received: 12 April 2012 / Revised: 19 April 2012 / Accepted: 19 April 2012 / Published online: 8 May 2012

Abstract Annealed thin layers of gold with large mono-crystalline areas were treated with OH˙ radicals generated in an electrochemical Fenton reaction. The morphological changes observed with ex situ atomic force microscopy in non-contact mode and grazing incidence X-ray diffractometry show that the grain boundaries, and generally the non-{111} planes, are the loci of highest reactivity, i.e., the places where the gold dissolution is much faster than on the {111} planes.

Keywords Mono-crystalline gold · OH˙ radicals · Non-contact AFM · STM · Electrochemical Fenton reaction · XPS · X-ray diffraction

Dedicated to Dr. Nina Fjodorovna Zakharchuk on the occasion of her 75th birthday.

U. Hasse (✉) · G. Sievers · F. Scholz
Institute for Biochemistry, University Greifswald,
Felix-Hausdorff-Str. 4,
17489 Greifswald, Germany
e-mail: Hasse@uni-greifswald.de

K. Fricke
Leibniz Institute for Plasma Science
and Technology e.V. (INP Greifswald),
Felix-Hausdorff-Str. 2,
17489 Greifswald, Germany

D. Dias
Departamento de Química, Universidade Federal de Santa Maria,
C. P. 5051, 97105-970 Santa Maria, RS, Brazil

H. Wulff
Institute of Physics, University Greifswald,
Felix-Hausdorff-Str. 6,
17489 Greifswald, Germany

Introduction

Previously, we have reported on the interaction of OH˙ radicals with the surface of poly-crystalline noble metals (Au, Pt, Pd, and Ag) [1–3] and glassy carbon [4]. Particular attention was given to alterations of the surface morphology, the electrocatalytic properties, and the properties of the surfaces in nucleation growth of metal deposition [1, 5]. Yang et al. have investigated the influence of OH˙ radicals on gold nano-particles in respect to surface alterations and electrocatalytic activity [6]. Following the studies of poly-crystalline metal surfaces, it is of course necessary to understand how OH˙ radicals affect mono-crystalline surfaces, which can be rather easily produced by flame annealing or heat treatment of thin layers of gold, vapor-deposited on borosilicate glass [7, 8]. In the present study, mono-crystalline surfaces of such gold layers were prepared by heat treatment in an oven under nitrogen atmosphere. The morphological changes were followed by ex situ non-contact atomic force microscopy (AFM), taking careful attention to image exactly the same sites of the surface before and after the treatment with OH˙ radicals.

Experimental

Equipment

The AFM measurements were performed with a DualScope 95-50, DME, Denmark, with the Software DME Scan Tool Version 1.2.1.0 (non-contact mode). All STM measurements were performed with a NanoScope 1.0 with its Software NANOSCOPE E Version 4.23r3 at room temperature and under atmospheric pressure. For OH˙ radical generating a PGSTAT 101 and for cyclic voltammetry measurements of thiol desorption a Computrace Model 757 VA, both Methrom, Switzerland, were used. An Ag/AgCl (3 M KCl) reference electrode was used (E=0.208 V vs. SHE) in the electrochemical experiments.

XPS measurements were performed with an Axis Ultra, Kratos Analytical, Manchester, UK. Data acquisition and processing were carried out using CasaXPS software, version 2.14dev29 (Casa Software Ltd., UK). The chemical surface composition was examined by XPS using an AXIS Ultra DLD electron spectrometer. Wide scans were recorded by means of monochromic Al K_α excitation (1,486.6 eV) with a medium magnification (field of view 2) lens mode and by selecting the slot mode, providing an analysis area of approximately 250 µm in diameter, operating at a pass energy of 80 eV. Charge neutralization was implemented by low energy electrons injected into the magnetic field of the lens from a filament located directly atop the sample.

X-ray diffraction was used for the characterization of the thin gold films. Thin poly-crystalline films can be advantageously studied in a highly asymmetric Bragg case (grazing incidence X-ray diffractometry (GIXD)) to obtain information from near-surface region of a sample [9]. For the analysis of layers, the information depth of X-rays is an important factor, in particular, if gradients of structure parameters occur in the films. The film information depth Y strongly depends on the film thickness x_o, the mean absorption coefficient μ and of course on the incidence angle ω:

$$Y = \frac{1}{\mu Z}(1 - \exp(-x_0 Z)) \text{ with } Z = \frac{1}{\sin\omega} + \frac{1}{\sin(2\theta - \omega)}$$

The X-ray parameters measured represent only absorption weighted effective parameters, different from the true values in the film.

The Au films were characterized after annealing and then after OH˙ radical attack by GIXD (incidence angle ω=0.5°, 1°, and 2°) to determine the phase composition, domain sizes, and crystallite orientation of the crystalline materials in the films. GIXD was performed using a Siemens D5000 diffractometer equipped with a special parallel beam attachment (plate collimator). Cu K_α radiation (40 kV, 40 mA) was used. The scanned 2θ range was 30° to 50°.

Chemicals

Iron(III) sulfate, ethanethiole, hydrogen peroxide, and sulfuric acid were all of p.a. quality and purchased from Merck, Germany. The gold on glass samples were purchased from Schröer GmbH, Lienen, Germany. These plates are made of

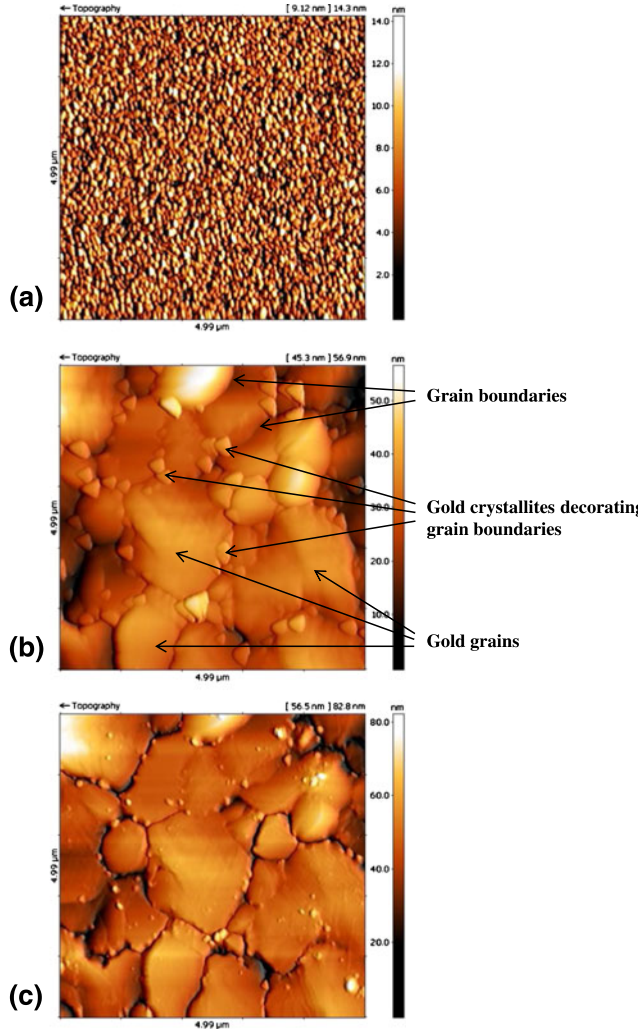

Fig. 1 Atomic force micrographs of the gold surface **a** before annealing, **b** after annealing (and before exposure to OH˙ radicals), and **c** after 30 s OH˙ generation

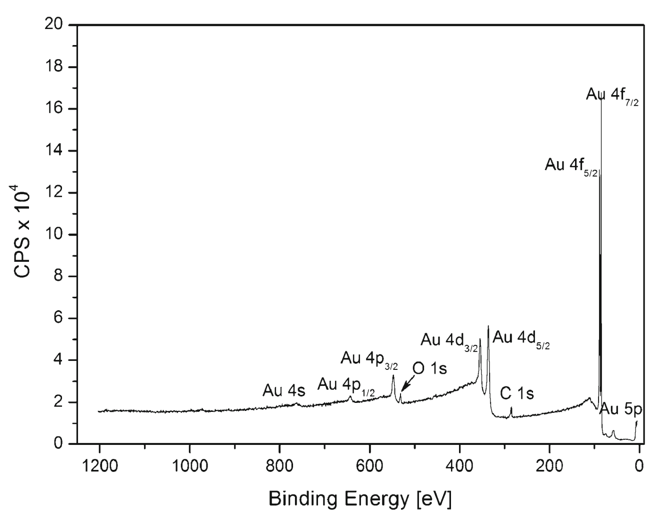

Fig. 2 XPS spectrum of an annealed gold surface (*cps* counts per second). Recording conditions: see "Experimental"

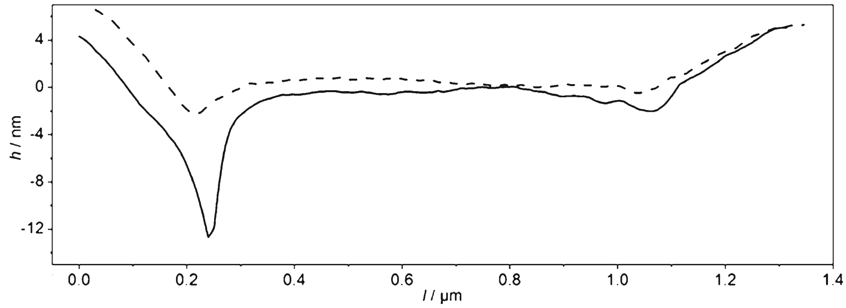

Fig. 3 Section analyses of AFM images. The *dashed line* depicts the profile before and the *solid line* after OH˙ radical attack

borosilicate glass with a layer of metallic chromium and a 250-µm thick gold layer on top.

Sample preparation

The gold on glass plates were carefully washed with isopropanol and finally with water. The plates were heated under nitrogen atmosphere up to 750 °C within 15 min, then kept for 20 min at 750 °C, and finally cooled down to room temperature in a stream of nitrogen gas.

OH˙ radical generation

The OH˙ radicals were generated by the electrochemical Fenton reaction. For this, an oxygen saturated solution was used which contained 0.1 mol L^{-1} Fe(II) sulfate and 0.1 mol L^{-1} sulfuric acid. Following a literature procedure [10], the OH˙ radical generation was performed by applying a constant current of 10 mA.

Results and discussion

Figure 1a shows an AFM micrograph of the pristine surface of a thin layer of gold, and Fig 1b shows the surface after annealing. Clearly, after the annealing, the grain boundaries are decorated by well-defined gold crystallites. XPS proved that these small crystallites were indeed gold (only minute surface contaminations (carbon and oxygen) were present) (cf. Fig. 2). Similar small crystallites have been observed earlier by other authors using much longer annealing times (up to 35 h) [11] and in these experiments, the small crystallites consisted of chromium which had diffused towards the grain boundaries from underneath the gold layer. It is important to note that in our experiments these crystallites were of pure gold, i.e., no chromium could be detected by XPS and GIXD in the upper layers. XRD in Bragg–Brentano geometry clearly proves the formation of Au–Cr solid solutions near substrate.

Figure 1c shows the effect of OH˙ radicals on the same surface area after 30 s of OH˙ radical attack. It is obvious that the small gold crystallites at the grain boundaries had nearly completely dissolved. Moreover, a section analysis revealed that the grooves along the grain boundaries had deepened (Fig. 3). In some places, the increase in depth approached 200 %. It must be kept in mind, however, that these grooves might be even deeper, as it cannot be excluded that the cantilever tip was too large to record the real depth. In contrast to the small crystallites and grain boundaries, the mono-crystalline areas are obviously not affected. Figure 4 depicts an overlay of Fig. 1b, c. It shows impressively the dimension of the dissolution along the grooves between the mono-crystalline grains and the very pronounced dissolution of the small gold crystallites decorating the grain boundaries.

What we here call *grain boundaries* of the gold crystals, as imaged by AFM, are in fact complicated *triple phase junction lines* at which two gold crystals and an aqueous solution (in the case of the OH˙ attack) or air (in the AFM measurements) meet each other. Of course, they are also not two-dimensional, but three–dimensional. When such grain boundaries are considered, line tension may also come into play. Line tension, introduced by Gibbs, is the work associated with expanding the length of a *two-phase junction line*, and in most real cases, a *three–phase junction line* [12, 13]. In contrast to surface tension, which is always positive (as otherwise the interface would not be stable), it is still a matter of debate whether line tensions can be negative. Figure 5 depicts schematically a cut through the surface of

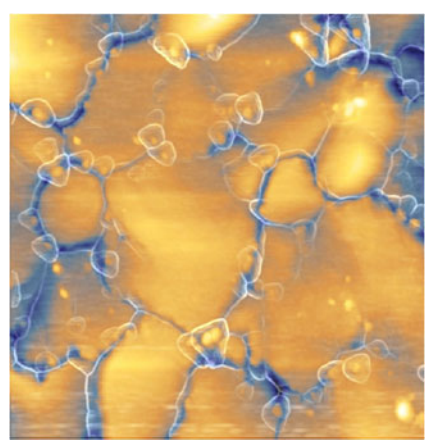

Fig. 4 Overlay of Fig. 1b, c to demonstrate the original positions and sizes of the dissolved parts. Color coding: *yellow* smallest changes, *blue* largest changes, and *white lines* initial position of interfaces and grain boundaries

Fig. 5 Schematic cut through the boundary between gold grains

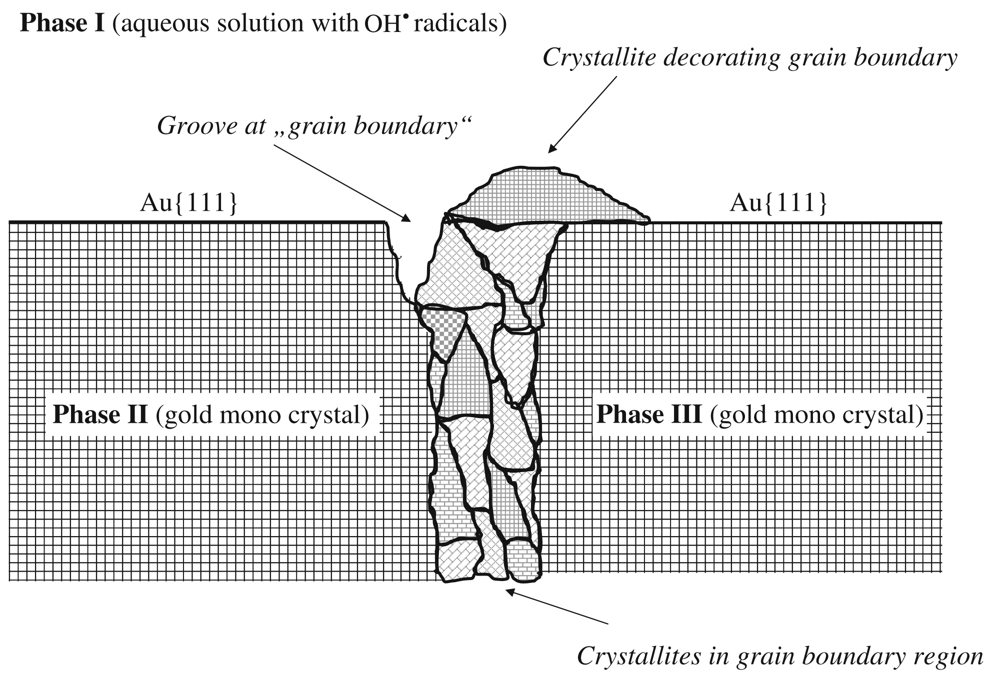

the annealed gold layer. The Au grains are oriented in such way that the Au{111} crystal planes are on top. At the grain boundaries, small grooves separate the grains and the "gaps" between the large mono-crystals are filled with small crystallites, some of which decorate the grain boundaries on the surface. Of course it is possible that the interfaces between the gold crystals are in fact *interphases* [14], but we have no information about this. The schematic structure depicted in Fig. 5 explains all the experimental findings (AFM, X-ray diffraction, and electrochemistry) which are reported here. In a recent experimental study, it has been shown that *triple-phase junctions* (tpjs) on the surface of nano-crystalline zirconia thin films form pits, and these tpjs have zero to positive energies (no negative energies were found) [15]. Note that a tpj is the location where three crystals meet in the surface plane. They should not be confused with tpj lines. Figure 1b also exhibits a number of tpjs forming pits, and a closer look at Fig. 4 reveals not only that the grain boundaries are the locations of the most severe gold dissolution by OH˙ radicals, but especially the tpj points, i.e., the spots were three grains meet. Figure 4 also shows that the grain boundaries of the *small crystallites* considerably shrink, whereas the length of the boundaries between *the larger gold grains* remain more or less the same. Of course, this is due to the geometry. The interesting question as to the extent by which the dissolution is affected by line tension cannot yet be answered.

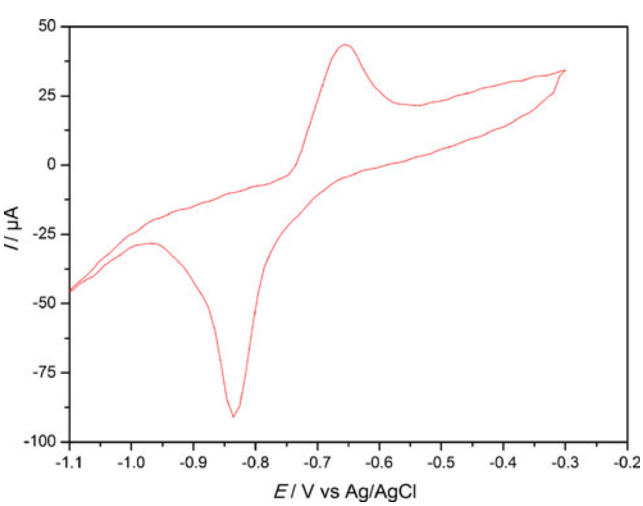

Fig. 6 Cyclic voltammogram of ethanthiol (0.6 mM) in alkaline solution (0.5 M NaOH) on a Au{111} gold electrode at a scan rate of 400 mV s^{-1}

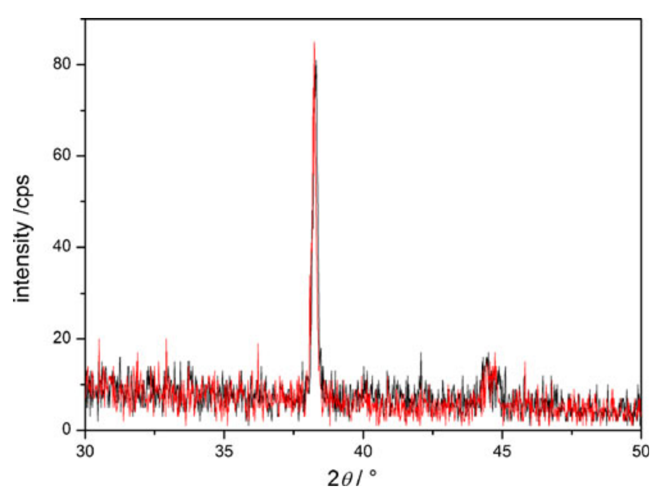

Fig. 7 X-ray pattern measured at an incidence angle of ω=0.5° before (*black*) and after (*red*) OH˙ radical attack (*cps* counts per second)

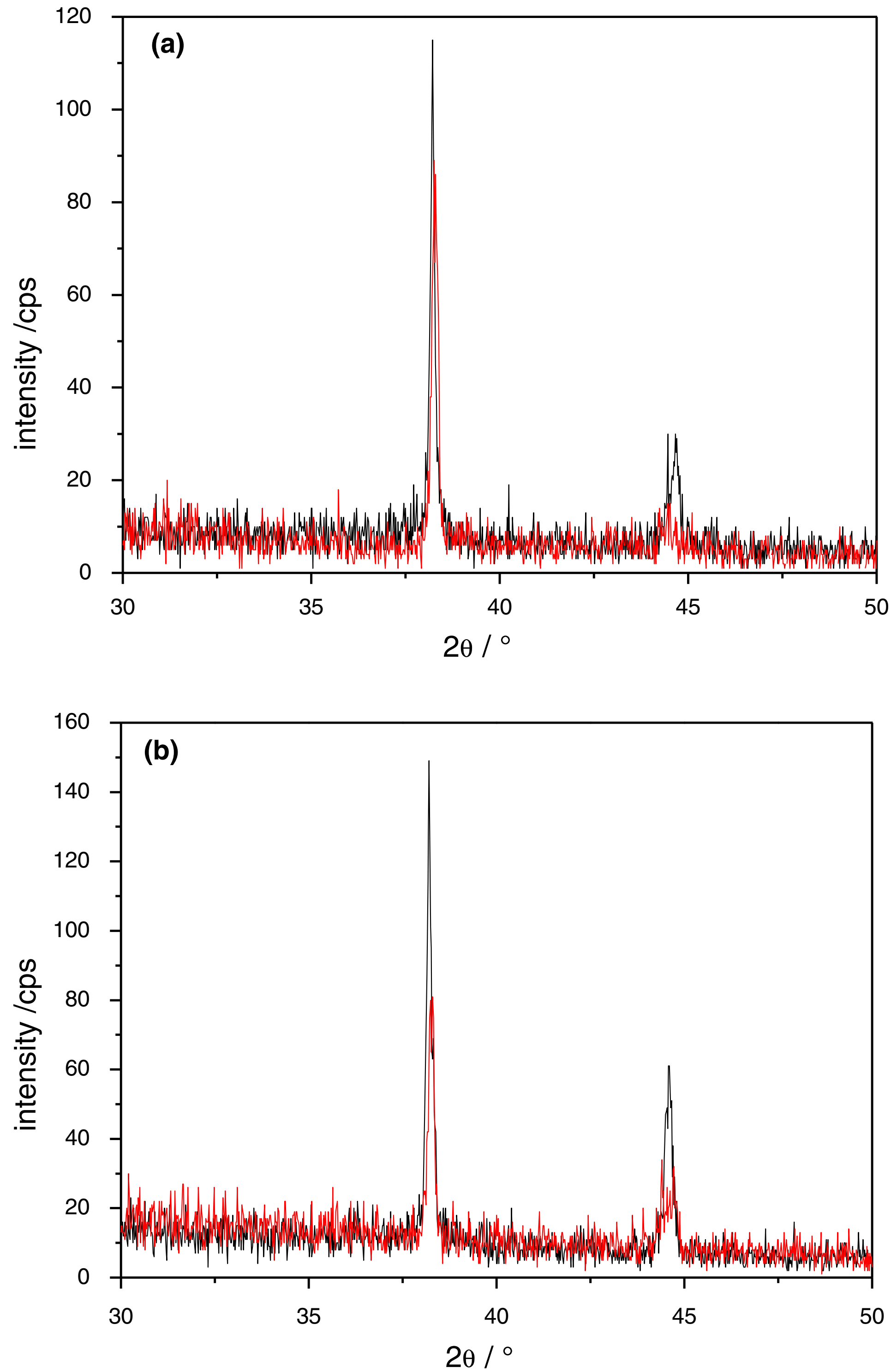

Fig. 8 X-ray pattern measured at an incidence angle of ω=1° **a** and ω=2° **b** before (*black*) and after (*red*) OH˙ radical attack (*cps* counts per second)

Yang et al. have shown that the potential of the electrochemically reductive desorption of thiols from gold depends on the crystal planes of the gold electrodes [16]. Figure 6 shows a cyclic voltammogram of ethanethiol on the annealed gold electrode (geometric surface area of the electrode, 121 mm^2 and scan rate, 400 mV s^{-1}). The peak at −0.835 V vs. Ag/AgCl represents the reductive desorption of ethanethiol from the Au{111} crystal plane. No other peak was observed, so that it can be concluded that really the Au {111} planes dominate on the surface of the annealed gold electrode, as it was reported in numerous other papers [17, 18].

This result was corroborated by the X-ray diffraction data. Figure 7 shows the X-ray pattern measured at an

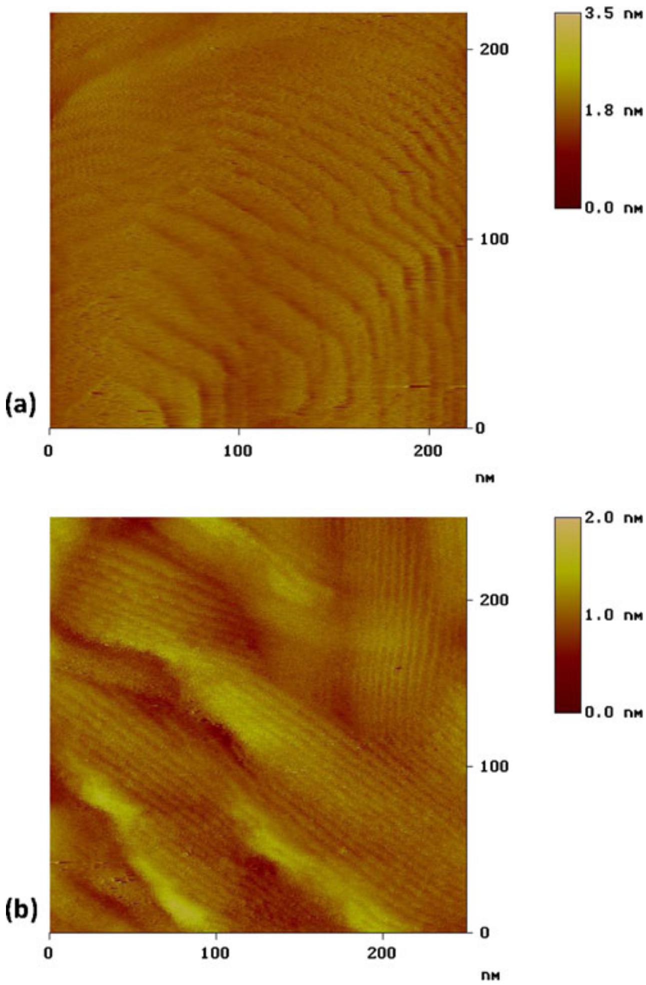

Fig. 9 STM micrographs **a** of an Au crystallite with crystal plane steps and **b** of reconstructed Au{111}planes at another location of the same crystallite

incidence angle of ω=0.5° before and after the $\mathrm{OH}^{\cdot}$ radical attack. The information depth Y calculated according to equation (see "Experimental") is 21 nm. No difference between these two X-ray patterns can be observed. Both X-ray patterns exhibit poly-crystalline Au with strongly preferred {111} orientation. The {111} reflection profiles are very narrow and correspond to domain sizes of 55 nm (calculated from the Fourier transforms [8]). That means the $\mathrm{OH}^{\cdot}$ radical attack takes place predominantly at small Au crystallites surrounding the monocrystalline particles and along grain boundaries or dislocations.

At increasing incidence angles (for ω=1°, Y=40 nm and for ω=2°, Y=79 nm), i.e., by studying thicker layers, the X-ray patterns measured before $\mathrm{OH}^{\cdot}$ radical attack show a larger contribution of small statistically distributed crystallites (Fig. 8). This can easily be explained with the Scheme in Fig. 5 because in that case a larger number of small crystallites situated between the mono crystals contributes to the diffraction pattern. After the $\mathrm{OH}^{\cdot}$ radical attack (Fig. 8), the contribution of the small crystallites to the X-diffractogram is diminished because the small crystallites are subject to a preferential dissolution as it is was also found in the AFM studies.

Grain boundary corrosion is certainly one of the most intensively studied topics [19, 20] of corrosion. There are several reasons why an increased corrosion rate may be observed at grain boundaries, for example a high defect concentration, the specific nature of the defects at grain boundaries, composition differences between adjacent grains and resulting potential differences, the existence of inter*phases*, stress, etc. In the case of the annealed gold surface, composition and thus potential differences between the grains can be almost ruled out. Certainly, minute traces of metal atoms diffusing from the chromium base cannot be completely ruled out, as the sensitivity of XPS is insufficient to detect such traces. Waibel et al. [21] have studied the electrochemical deposition of platinum at the same kind of annealed gold electrodes, and they found that Pt deposition starts at terraces. The grain boundaries were not imaged by these authors. In our experiments, the large rather flat surface planes of the grains are {111} faces, and the grain boundaries are predominantly non-{111} faces. A very careful examination of the {111} faces did not show any detectable changes of the position of the terraces, so that it has to be concluded that the $\mathrm{OH}^{\cdot}$ radicals mainly affect the grain boundaries, either because these are non-{111} faces, or because they have a higher defect concentration. In principle the dissolution of gold by $\mathrm{OH}^{\cdot}$ radicals can be envisaged to occur as a bimolecular reaction $\mathrm{OH}^{\cdot} + \mathrm{Au} \rightarrow \mathrm{OH}^{-} + \mathrm{Au}^{+}$. However, bearing in mind that gold is a metal, it may be better to understand the corrosion on the basis of the electrochemical theory of a (local) galvanic cell, i.e., $\mathrm{OH}^{\cdot}$ radicals being reduced at some locations, and Au atoms being oxidized at others. This means that $\mathrm{OH}^{\cdot}$ radicals can be oxidized on the entire gold surface, wherever it happens that they arrive by diffusion to the surface. The dissolution, i.e., the anodic oxidation of gold, however, will preferably occur at locations where that process has the largest driving force. Rather contradictory data of the work functions were reported for the different gold planes [22–24]. Furthermore, these data were determined by measurements in high vacuum, whereas our measurements relate to gold in contact with aqueous electrolyte solutions. Thus it is impossible to make differences in work functions responsible for the different rates of dissolution. What can be clearly stated is just the experimental result that the well-developed {111} faces exhibit no or no detectable corrosion, whereas the non-{111} faces, i.e., grain boundary grooves and also the almost vertical side planes of the small Au crystallites, are rather quickly dissolving.

Figure 9 shows two STM micrographs of two different locations of one small crystallite (one of the crystallites decorating the grain boundaries in Fig. 1b) at a grain boundary. In

Fig 9a, steps of well-developed crystal planes are visible. In Fig 9b, the well-known patterns of a reconstructed Au{111} plane are visible. The section analysis (not shown here) gives an average corrugation length of 5.6 nm. This value is in rather good agreement with the ($\sqrt{3} \times$ `22) reconstruction with a corrugation length of 6.3 nm [25]. Kolb et al. have shown that especially in the case of flame annealing, this kind of reconstruction can take place with a herringbone alignment or simple parallel stripes [26]. The fact that pronounced stepped structures and also the ($\sqrt{3} \times$ `22) reconstruction was detected on the surface of the small gold crystallites indicates that local stress during their genesis or, more likely, during the cooling period has affected these crystallites. Interestingly, the large Au{111} planes of the Au grains, did not show these reconstruction and step features. Possibly, these step and reconstruction features of the small crystallites are responsible for their high dissolution rate.

Conclusions

We could show that small gold crystallites grow during the annealing process of a thin gold layer, and decorate the grain boundaries of the well-developed Au{111} crystal planes. $OH^{\cdot}$ radicals generated in an electrochemical Fenton reaction, lead to a fast dissolution of small gold particles surrounding the mono-crystalline Au particles. The big Au{111} planes are not or not detectably affected. These features are typical for grain boundary corrosion. In this study it was not possible to pinpoint the real reasons for that process, and one can only speculate that different values of the work function, defect concentrations, mechanical stress, etc. may be responsible. Here, a comparison of the present results with those of our earlier electrochemical studies is very interesting: in previous studies, we have shown that at poly-crystalline gold, $OH^{\cdot}$ radicals (1) preferably knock out active sites of electrocatalytic reactions (oxygen and hydroquinone reduction), and (2) they also knock-out the active sites for platinum deposition [1–3]. Hence, there is the possibility that the active sites for electrocatalysis and electrodeposition may be non-Au{111} faces, i.e., grain boundaries or locations with high defect concentrations.

Acknowledgments The authors are very thankful to Professor Stephen Fletcher, Loughborough University, UK, for a detailed discussion of the results and especially for raising the question of line tension. F.S. and U.H. acknowledge the funding of the AFM instrumentation by the European Regional Development Fund (EFRE). G.S. acknowledges support by a fellowship of the Alfried Krupp Wissenschaftskolleg Greifswald. D.D. acknowledges support by CAPES Brazil and DAAD.

References

1. Nowicka AN, Hasse U, Hermes M, Scholz F (2010) Angew Chem Int Ed 49:1061
2. Nowicka AN, Hasse U, Donten M, Hermes M, Stojek ZJ, Scholz F (2011) J Solid State Electrochem 15:2141
3. Sievers G, Hasse U, Scholz F (2012) J Solid State Electrochem 16:1663
4. Rapecki T, Nowicka AN, Donten M, Scholz F, Stojek Z (2010) Electrochem Commun 12:1531
5. Nowicka AN, Hasse U, Sievers G, Donten M, Stojek Z, Fletcher S, Scholz F (2010) Angew Chem Int Ed 49:3006
6. Dutta G, Yang H (2011) Electrochem Commun 13:1328
7. Dakkouri AS, Randler R, Kolb DM (1997) Structure and dynamics of metal single crystal surfaces. In: Korzeniewski C, Conway BE (eds) Proc symp: the electrochemical double layer, vol 97–17. The Electrochem Soc, Pennington, pp 13–32
8. Hammiche A, Webb RP, Wilson IH (1994) Vacuum 45:569
9. Wulff H, Steffen H (2008) Characterization of thin films. In: Hippler R, Kersten H, Schmidt H, Schoenbach KH (eds) Low temperature plasmas. Wiley, Berlin, p 329
10. Oturan MA, Guivarch E, Oturan N, Sires I (2008) Appl Catal, B 82:244
11. Munitz A, Komem Y (1980) Thin Solid Films 71:177
12. Tadmor R (2008) Surf Sc 602:L108–L111
13. Amirfazli A, Neumann AW (2004) Adv Coll Interf Sc 110:121–141
14. Sutton AP, Balluffi RW (1995) Interfaces in crystalline materials. Clarendon Press, Oxford
15. Kim H, Xuan Y, Ye PD, Narayanan R, King AH (2009) Acta Materialia 57:3662–3670
16. Yang DF, Wilde CP, Morin M (1996) Langmuir 12:6570
17. Watanabe MO, Tanaka K, Sakai A (1990) J Vac Sci Technol, B 9:924
18. Porath D, Goldstein Y, Grayevsky A, Millo O (1994) Surf Sci 321:81
19. Toedt F (1961) Korrosion und Korrosionsschutz. Walter de Gruyter, Berlin, p711
20. Kaesche H (1990) Die Korrosion der Metalle. Springer, Berlin, p 353
21. Waibel HF, Kleinert M, Kibler LA, Kolb DM (2002) Electrochim Acta 47:1461
22. Jakobi K (1994) Surface core-level shift data 3.1.2.5, electronic and vibrational properties. In: Chiarotti G (ed) Landolt–Börnstein—group III condensed matter numerical data and functional relationships in science and technology, vol 24b. Springer, Berlin
23. Michaelson HB (1977) J Appl Phys 48:4729
24. Skriver HL, Rosengaard NM (1992) Phys Rev B 46:7157
25. Dakkouri AS, Kolb DM (1999) Reconstruction of gold surfaces. In: Wieckowski A (ed) Interfacial electrochemistry: theorie, experiment and applications. Marcel Dekker, New York, p 151
26. Kolb DM, Dakkouri AS, Batina N (1995) The surface structure of gold single-crystal electrodes. In: Gewirth AA, Siegenthaler H (eds) Nanoscale probes of the solid/liquid interface. NATO ASI, vol E. Kluwer, Dordrecht, p 263